Available online at www.sciencedirect.com
SCIENCE DIRECT
International Journal of Heat and Mass Transfer 49 (2006) 3807–3818
International Journal of HEAT and MASS TRANSFER
www.elsevier.com/locate/ijhmt

Natural convection heat transfer enhancement using adiabatic block: Optimal block size and Prandtl number effect

Prasad Bhave [a], Arunn Narasimhan [a,*], D.A.S. Rees [b]

[a] Heat Transfer and Thermal Power Laboratory, Department of Mechanical Engineering, Indian Institute of Technology Madras, Chennai 600 036, India

[b] Department of Mechanical Engineering, University of Bath, Claverton Down, Bath BA2 7AY, UK

Received 30 September 2005; received in revised form 2 February 2006
Available online 30 June 2006

Abstract

Numerical methods are used to solve the finite volume formulation of the two-dimensional mass, momentum and energy equations for steady-state natural convection inside a square enclosure. The enclosure consists of adiabatic horizontal walls and differentially heated vertical walls, but it also contains an adiabatic centrally-placed solid block. The aim of the study is to delineate the effect of such a block on the flow and temperature fields. The parametric study covers the range $10^3 \leqslant Ra \leqslant 10^6$ and is done at three Pr namely, 0.071, 0.71 and 7.1. In addition the effect of increasing the size (characterized by the solidity Φ) of the adiabatic block is ascertained. It is found that the wall heat transfer increases, with increase in the Φ, until it reaches a critical value $\Phi = \Phi_{OPT}$, where the wall heat transfer attains its maximum. Further increases in the block size beyond Φ_{OPT}, reduces the wall heat transfer, for as the block size becomes larger than the conduction dominant core size it reduces the thermal mass of the convecting fluid. A steady-state heat transfer enhancement of 10% is observed for certain Ra and Pr values. Useful correlations predicting this optimum block size and the corresponding maximum heat transfer as a function of Ra and Pr are proposed; these predict within $\pm 3\%$, the numerical results.

1. Introduction

Natural convection in side wall heated square cavities has been studied widely for its various applications in engineering and geo-physical systems [1–4]. Heat transfer in an enclosure with a centered body also finds direct applications in the construction of buildings with natural cooling flow. In such enclosure configurations there is a stagnant core of the fluid that does not participate in the convection heat transfer across the enclosure side walls [5]. In fact, the presence of this stagnant core impedes the convective flow inside the enclosure by its vertical heat conduction potential and it reduces the average steady-state wall heat transfer crossing the enclosure side walls, which are kept at a fixed temperature difference. If this vertical heat conduction in the core is prevented completely, a corresponding steady-state heat transfer enhancement may be observed across the enclosure side walls kept at a fixed temperature difference. For instance, the work reported in [5], deals with the qualitative effects of a centered solid body of different conductivities on the enclosure convection heat transfer. However, the exact quantification of the resulting heat transfer increase and the effect of different Prandtl numbers were not studied in the work. Convection in enclosures containing blocks has gained recent research significance as a means of heat transfer enhancement [6], for delineating porous medium behavior [7] and for analyzing enclosure convection with finite size conducting blocks [8]. Steady natural convection processes have been investigated in [9] when a temperature difference exists across the enclosure and, at the same time, a conducting body generates heat within the enclosure. A comprehensive numerical study is performed in [10] to investigate the transient heat transfer and flow characteristics of the natural convection of three

* Corresponding author. Tel.: +91 44 225 74696; fax: +91 44 225 78501.
E-mail addresses: arunn@iitm.ac.in (A. Narasimhan), ensdasr@bath.ac.uk (D.A.S. Rees).

0017-9310/$ - see front matter © 2006 Elsevier Ltd. All rights reserved.
doi:10.1016/j.ijheatmasstransfer.2006.04.017

Nomenclature

A	total area of the enclosure, m^2
B_{MAX}	maximum length scale used to define the stagnant core in the X direction
c_P	specific heat of the fluid, J/kg-K
Case 1	results pertaining to when the adiabatic block is absent
Case 2	results pertaining to when the adiabatic block is present
H	characteristic dimension of the square enclosure, m
k_s	thermal conductivity of the solid, W/m-K
k_f	thermal conductivity of the fluid, W/m-K
K	ratio of fluid to solid (block) thermal conductivity k_f/k_s, Table 2a and b
L	characteristic dimension of the square adiabatic block, m
Nu	Nusselt number based on enclosure length scale, Eq. (10)
p	pressure, Pa
P	dimensionless pressure, Eq. (5)
Pr	Prandtl number, Eq. (6)
q''	heat flux crossing the enclosure side wall, W/m^2
Q	heat flux enhancement parameter, q''_1/q''_2
Ra	Rayleigh number based on H, Eq. (6)
T	temperature, K
u, v	local velocities along x and y directions, m/s
U, V	dimensionless fluid velocities, uH/α, vH/α
W_{MAX}	maximum length scale used to define the stagnant core in the Y direction
W_{MIN}	minimum length scale used to define the stagnant core in the Y direction
X, Y	dimensionless Cartesian coordinates, x/H, y/H

Greek symbols

α	diffusivity of the fluid, $k/\rho c_P$, m^2/s
δ	local hydrodynamic boundary layer thickness, ($\sim HPr^{1/2}Ra^{-1/4}$, cf. [4] p. 224)
δ_T	local thermal boundary layer thickness, ($\sim HRa^{-1/4}$, cf. [4] p. 223)
ρ	density of the fluid, kg/m^3
θ	dimensionless temperature
Φ	solidity of the enclosure $= A_b/A = L^2$, Fig. 1

Subscripts

1	Case 1, without adiabatic block
2	Case 2, with adiabatic block
b	adiabatic block
bottom	bottom face of the adiabatic block
c	cold value
h	hot value
top	top face of the adiabatic block

different fluids in a vertical square enclosure within which a centered, square, heat-conducting body generates heat. Heat transfer enhancement within enclosures has also been addressed in [11,12] and in [13], without and with partitions respectively.

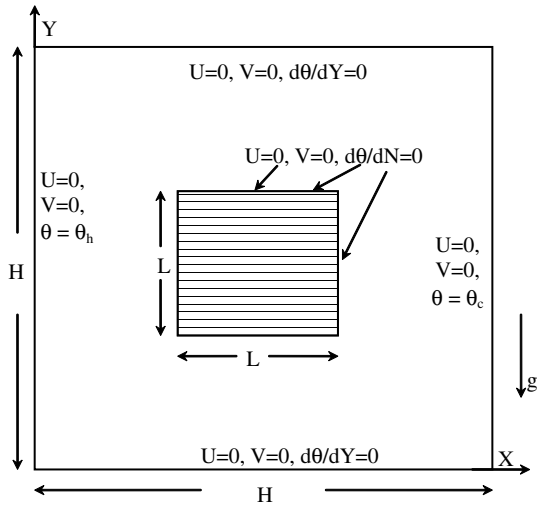

Fig. 1. Schematic of the problem with the domain and boundary conditions used (a) Case 1: square enclosure with top and bottom walls horizontal and side walls differentially heated and (b) Case 2: the same square enclosure with an adiabatic block placed at the centre.

In the present paper, we investigate the effect on the steady-state natural convection heat transfer enhancement of a centrally-placed adiabatic block within a differentially heated square cavity with a fixed temperature drop between the vertical walls.

2. Problem statement

The schematic of the problem is shown in Fig. 1. The square enclosure with adiabatic top and bottom walls is differentially heated from the sides, with the right hand wall held at the uniform temperature of T_c which is lower than T_h, the temperature of the left hand wall. Two cases are considered: Case 1, is the square enclosure of Fig. 1 minus the block and filled completely only with the convection fluid Case 2, shown in Fig. 1, is an enclosure with an adiabatic block placed at the center and the remaining area filled completely with the convecting fluid.

On defining a solidity parameter as the ratio of the area of the adiabatic block and that of the total enclosure volume, $\phi = A_b/A$, the effect of different values of ϕ on the steady-state heat transfer enhancement $Q = q''_1/q''_2$, is studied in detail for Ra lying between 10^3 and 10^6. This was done for the following three values of the Prandtl numbers, $Pr = 0.071$ (mercury), $Pr = 0.71$ (air) and $Pr = 7.1$ (water), thereby covering all the three limits of the Prandtl number

range ($Pr < 1$, ~1 and >1). A suitable theory is also developed, to predict the heat transfer between the enclosure side walls, in the presence of the adiabatic block.

3. Analysis

The governing two-dimensional mass, momentum and energy conservation equations of the problem are defined in non-dimensional form as follows:

$$\frac{\partial U}{\partial X}+\frac{\partial V}{\partial Y}=0, \tag{1}$$

$$U\frac{\partial U}{\partial X}+V\frac{\partial U}{\partial Y}=-\frac{\partial P}{\partial X}+Pr\left(\frac{\partial^2 U}{\partial X^2}+\frac{\partial^2 U}{\partial Y^2}\right), \tag{2}$$

$$U\frac{\partial V}{\partial X}+V\frac{\partial V}{\partial Y}=-\frac{\partial P}{\partial Y}+Pr\left(\frac{\partial^2 V}{\partial X^2}+\frac{\partial^2 V}{\partial Y^2}\right)+RaPr\theta, \tag{3}$$

$$U\frac{\partial \theta}{\partial Y}+V\frac{\partial \theta}{\partial Y}=\left(\frac{\partial^2 \theta}{\partial X^2}+\frac{\partial^2 \theta}{\partial Y^2}\right), \tag{4}$$

where the non-dimensional variables used in Eqs. (1)–(4) are defined as

$$U=uH/\alpha,\quad V=vH/\alpha,\quad X=x/H,\quad Y=y/H,$$
$$P=(p-p_\infty)H^2/\rho\alpha^2,\quad \theta=(T-T_c)/(T_h-T_c) \tag{5}$$

and

$$Ra=\rho g\beta H^3(T_{max}-T_{min})/\mu\alpha,\quad Pr=\nu/\alpha. \tag{6}$$

Further, in writing the conservation equations (1)–(4), the fluid properties are assumed to be constant except for the Boussinesq correction for the density in Eq. (3), where the gravity vector is assumed to act downward, as shown in Fig. 1 and p_∞ in Eq. (5) is a reference pressure. The appropriate boundary conditions (also shown in Fig. 1) used to solve Eq. (1)–(4) inside the enclosure are given as

$$\begin{aligned} &X=0,\quad U=V=0,\quad \theta=1;\\ &X=1,\quad U=V=0,\quad \theta=0,\\ &Y=0,\quad U=V=0,\quad \partial\theta/\partial Y=0;\\ &Y=1,\quad U=V=0,\quad \partial\theta/\partial Y=0. \end{aligned} \tag{7}$$

For the adiabatic block surface, the following generic boundary condition is used

$$U=V=0,\quad \text{and}\quad \partial\theta/\partial N=0, \tag{8}$$

where N is the direction normal to the surface of the adiabatic block in Fig. 1.

The numerical code used here was validated by comparing its results with benchmark solutions. More specifically the rate of heat transfer across the walls of the enclosure both with and without the adiabatic block in place was quantified using a wall surface averaged Nusselt number based on the enclosure length scale (H) which is defined as,

$$|Nu_h|=Nu_c=\int_0^1 \frac{\partial\theta}{\partial X}\,dY. \tag{9}$$

In addition the heat transfer enhancement caused by the presence of the adiabatic block was characterized using the ratio,

$$Q=Nu_{h,case2}/Nu_{h,case1}=q_2''/q_1'' \tag{10}$$

where the variables are defined in the nomenclature.

4. Numerical procedure

The numerical solution of the governing Eq. (1)–(4) was obtained by means of the control volume approach using the SIMPLER algorithm [14] with the QUICK scheme [15]. The results of the code used are first compared with the benchmark solutions [5,16,17] for a fluid of $Pr=0.71$ (air), and they were found to agree with an accuracy of 0.4%.

The comparison of the results, for both Case 1 and Case 2 is given in Table 1 and Table 2 (a and b), respectively. The chosen grid size was decided by a grid independence study for each Pr used. The results of such a test for $Pr=0.71$ is presented in Table 2a. From Table 2a it is observed that the relative error in Nu (calculated using Eq. (9)) has been reduced from 0.2% when going from a 80×80 grid to 100×100 grid to 0.04% while going from 100×100 to 120×120 grid. The final grid size used is a uniform 100×100 mesh, as shown in Fig. 2, using which all the results were generated for all three values of the Prandtl number. The grid is refined until the variation in the enclosure energy balance (found using the change in the Nusselt

Table 1
Validation of present Nu versus Ra results with published results for $Pr=0.71$

Ra	Present (100×100)	de Vahl Davies [16]	House [5]	Lage and Merrikh [17]
10^4	1.111	1.118	1.118	
10^5	2.24	2.243	2.254	2.244
10^6	4.502	4.519	4.561	4.536
10^7	8.85	8.8	8.923	8.86

Table 2a
Grid independence results for enclosure Nu (Eq. (9)) with a conducting block in Fig. 1

Ra	ϕ	K	80×80	100×100	120×120
10^6	0.5	0.2	4.648	4.645	4.643
10^6	0.5	5.0	4.341	4.338	4.337
10^7	0.9	0.2	2.321	2.326	2.325

Table 2b
Validation of the present Nu (Eq. (9)) results with a conducting block in Fig. 1

Ra	ϕ	K	Present	House [5]	Lage and Merrikh [17]
10^6	0.5	0.2	4.645	4.624	4.605
10^6	0.5	5.0	4.338	4.324	4.28
10^7	0.9	0.2	2.326	2.402	2.352

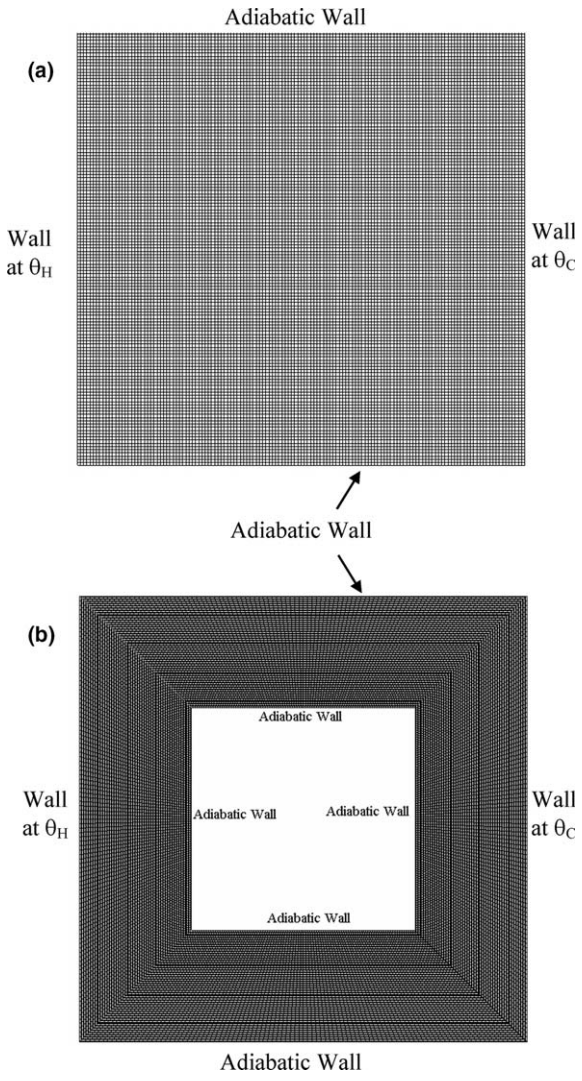

Fig. 2. Grid used for numerical simulations (a) Case 1 and (b) Case 2.

number obtained using Eq. (9)) was under 0.1%. The final convergence criterion between two successive iterations for the residual variation was set to 10^{-6} for both the continuity and momentum equations, and 10^{-8} for the energy equation.

5. Results and discussion

In all the streamline and isotherm plots there are 10 intervals represented by isolines with the labels 1–9 corresponding to tenths of the total variation between the respective maximum and minimum values. Fig. 3 shows the enclosure isotherms and streamlines when $Pr = 7.1$ for $10^3 \leqslant Ra \leqslant 10^6$ in the absence of the adiabatic block (Case1). The aim of this figure is to determine a definition of the size of the core of the fluid. The streamline $\psi = 0.9\psi_{max}$ in the centre of Fig. 3(b), (d), (f) and (h) indicates roughly the extent of the core of the fluid which is not participating in the convection of heat across the enclosure. In other words, the corresponding local velocity value would yield a local Peclet number ($=uH/\alpha$) of the order of one, suggesting in an order of magnitude sense, a conduction dominant zone. This conduction dominant maximum fluid core size is henceforth defined as a rectangular region (requiring at the most, only two length scales to define it), whose exterior boundary is the smallest one which contains completely the isoline,

$$\psi = 0.9\psi_{max}, \tag{11}$$

where ψ_{max} is the maximum value of the stream function in the enclosure. Although this definition is arbitrary, it is clear from the isotherm plots shown in Fig. 3(a), (c), (e) and (g) that heat conduction takes place vertically within this region and does not contribute to the steady-state wall-to-wall convection heat transfer. Therefore the effect of this conduction dominant core is to subtract a portion of the longitudinal wall to wall heat transfer by vertical cross conduction of heat (inferred from the horizontal nature of the isotherms in (a), (c), (e) and (g) in Fig. 3), hence reducing the net heat flux that can be transferred across the vertical walls, maintained at a fixed temperature difference.

Further, as the Ra increases (compare (a) and (b) with (c) and (d), for instance), the size of the stagnant core is observed to increase in size, especially in the horizontal direction. This is to be expected because it is known that, for $Pr > 1$, the boundary layer thickness δ near the isothermal vertical walls decreases with increasing values of Ra according to $\delta \sim HPr^{1/2}Ra^{-1/4}$ ([4] p. 224). The boundary layers coating the top and bottom adiabatic walls are not under the direct influence of a buoyancy force and exhibit only a weak 'growth' due to the increased flow rate for increasing Ra. In light of the above explanation, two length scales marked as B_{MAX} and W_{MAX} respectively are used in Fig. 3 to delineate the size of the core defined by $\psi = 0.9\psi_{max}$. However, it is worth noting that for $Ra = 10^5$ and 10^6, the $\psi = 0.9\psi_{max}$ curve is no longer of simple concave shape and it requires at least another length scale marked W_{MIN} in Fig. 3(e) through (h). Obviously, as seen from all the isotherms of Fig. 3, the magnitude of vertical heat conduction effect is governed more by W_{MAX} than by W_{MIN}.

Fig. 4 shows the effect of different values of Pr on the core size and shape when $Ra = 10^6$. Using the local velocities at $\psi = 0.9.\psi_{max}$, Eq. (11), from the simulation results for the case of $Pr = 0.071$ and $Ra = 10^6$, it was observed that the local Pe value is 2.4, clearly demarcating a conduction dominant core and also justifying the criterion defined in Eq. (11) to predict the same. It may also be observed that the core shape for $Pr = 0.071$, ((b) in Fig. 4) requires only two length scales, B_{MAX} and W_{MAX} respectively, while the cases for $Pr = 0.71$ and 7.1 ((d) and (f) respectively in Fig. 4) require the third value, W_{MIN}, to express their spatial extent. By comparing the cores for the all the three Pr values it is evident that the core size for $Pr = 0.71$ is less than that for $Pr = 7.1$. The core corresponding to $Pr = 7.1$ is the most stretched with B_{MAX}, W_{MAX} and W_{MIN} taking different values, while the core for the $Pr = 0.071$ value

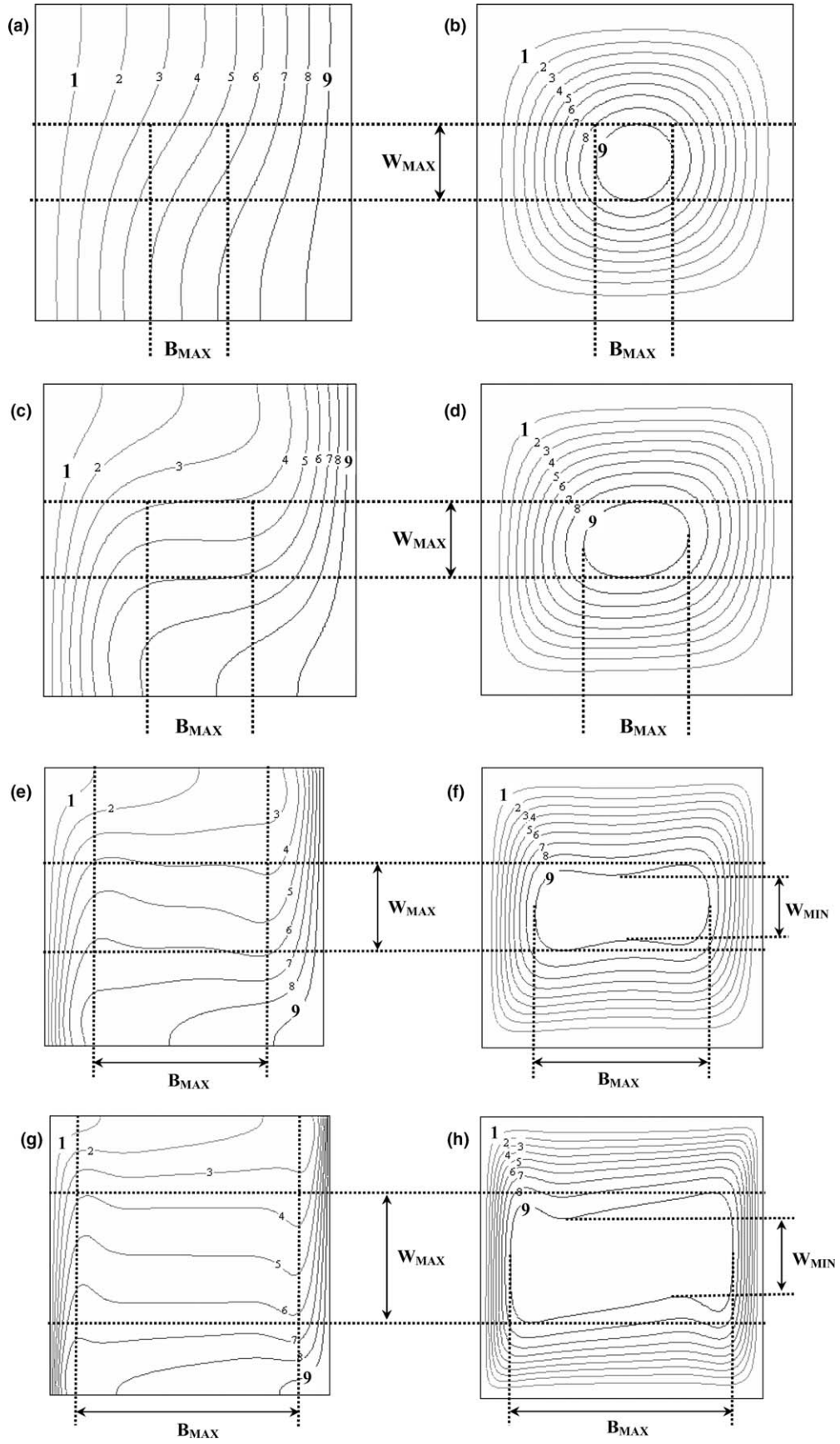

Fig. 3. Isotherms and streamlines respectively for Case 1 with $Pr = 7.1$ (a) and (b) $Ra = 10^3$, (c) and (d) $= 10^4$, (e) and (f) $= 10^5$, (g) and (h) $= 10^6$ respectively.

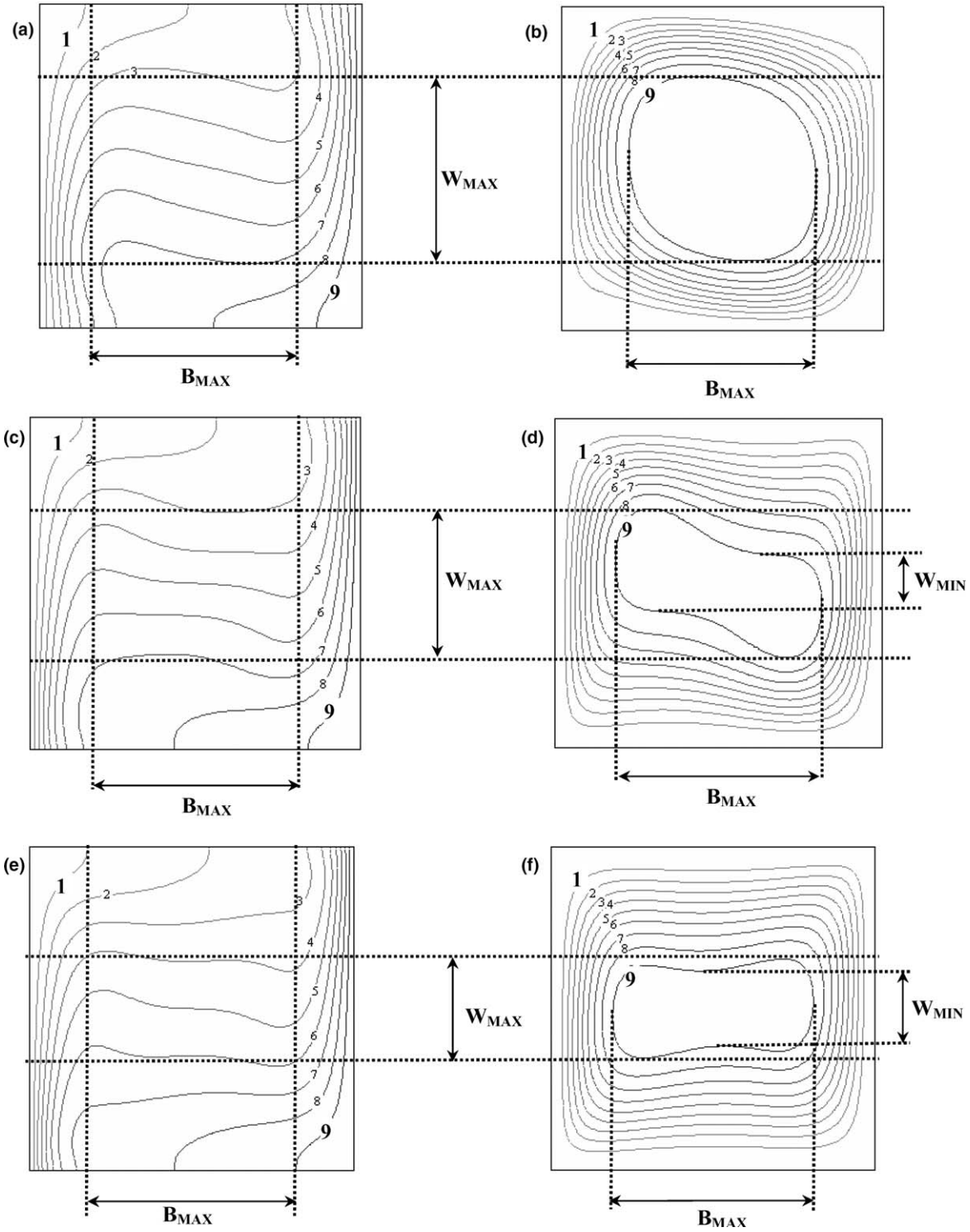

Fig. 4. The effect of different Prandtl numbers on the isotherms and streamlines for Case 1 with $Ra = 10^6$ (a) and (b) $Pr = 0.071$, (c) and (d) = 0.71, (e) and (f) = 7.1, respectively.

Table 3
Values of B_{MAX}, W_{MAX}, and W_{MIN} for several Ra and Pr

Ra	$Pr = 0.071$			$Pr = 0.71$			$Pr = 7.1$		
	B_{MAX}	W_{MAX}	W_{MIN}	B_{MAX}	W_{MAX}	W_{MIN}	B_{MAX}	W_{MAX}	W_{MIN}
10^4	0.296	0.284	0.284	0.334	0.252	0.252	0.34	0.248	0.248
10^5	0.586	0.574	0.308	0.63	0.452	0.236	0.618	0.31	0.236
10^6	0.737	0.746	0.389	0.804	0.656	0.298	0.792	0.464	0.276

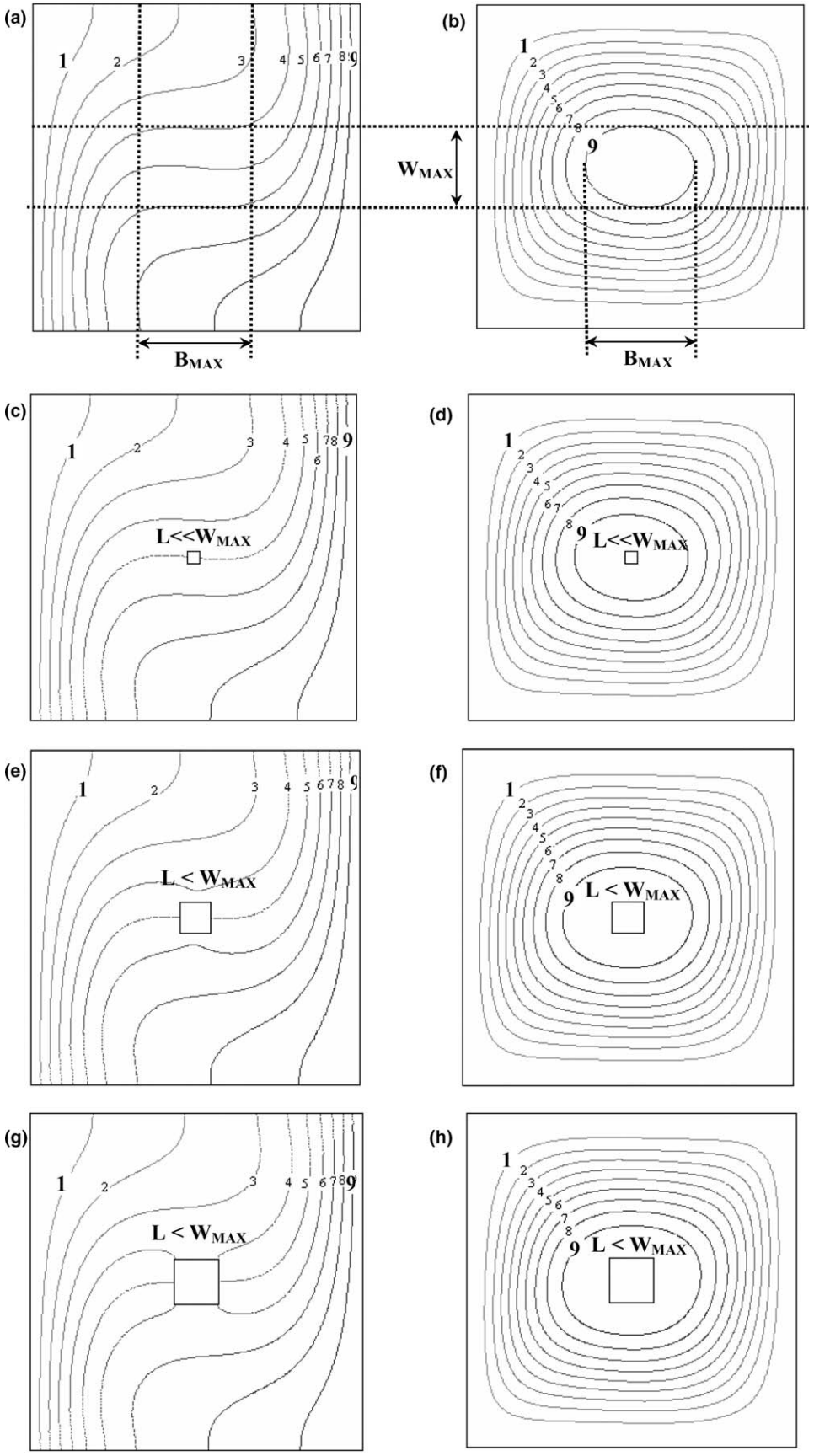

Fig. 5. Isotherms and streamlines respectively for $Ra = 10^4$ and $Pr = 0.71$: Case 1 in (a) and (b); Case 2 in (c) and (d) with Φ (%) = 0.16, (e) and (f) $\Phi = 0.9216$, (g) and (h) = 1.8, (i) and (j) $\Phi = 5$, (k) and (l) $\Phi = 10$, respectively.

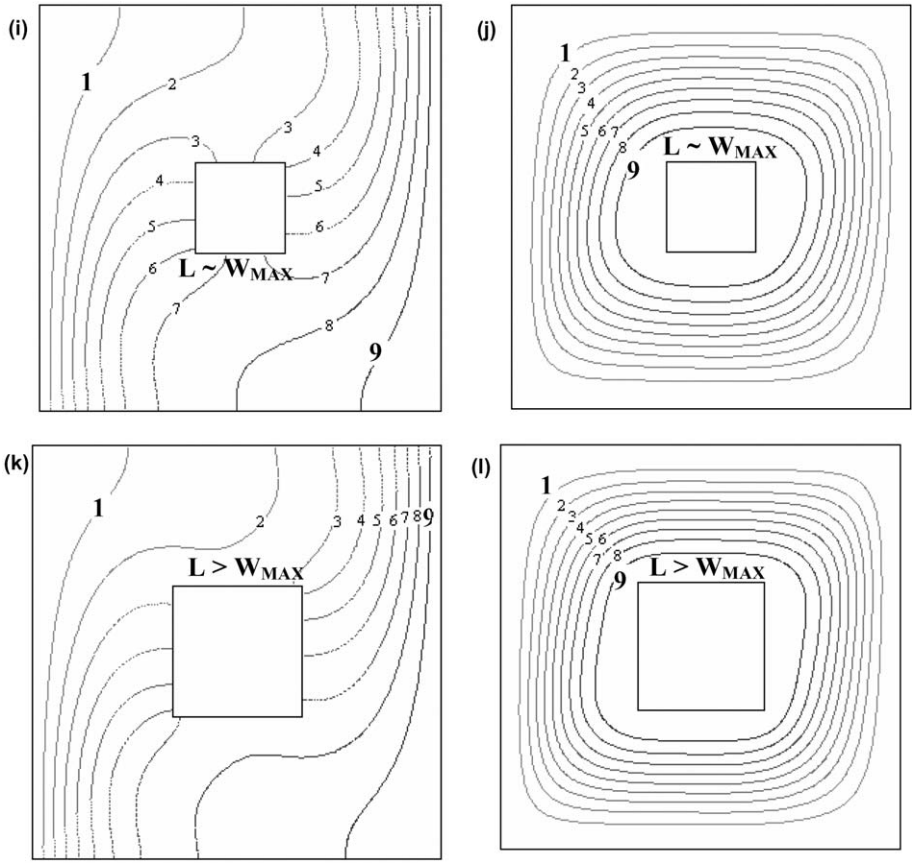

Fig. 5 (*continued*)

exhibits $B_{MAX} \sim W_{MAX}$, and is roughly square. This is also supported from the actual numerical values of these three length scales shown in Table 3, obtained from the numerical simulations for several Ra and Pr values.

It is worth keeping in mind that the length scale B_{MAX} of the cores shown in Fig. 4 may also be estimated in an order-of-magnitude sense using the length scales for the hydrodynamic and thermal boundary layers for the various values of Pr. For instance, when $Pr \geqslant 1$, $B_{MAX} \sim (H - 2\delta)$ and when $Pr < 1$, $B_{MAX} \sim (H - 2\delta_T)$. The B_{MAX} values given in Table 3 are consistent with these estimates.

The shape of the cores in Fig. 4, in particular for $Pr = 0.071$, suggests that one should use an adiabatic block of square shape in order to prevent the vertical heat conduction effect within convecting enclosures. Fig. 5 displays the isotherms and streamlines for $Ra = 10^4$ and $Pr = 0.71$ for an enclosure without the adiabatic block (Case 1) and with the adiabatic block (Case 2) for a variety of block sizes. The vertical heat conduction across the conduction dominant core seen in (a) and (b) is hardly altered by the presence of a block which is much smaller than the core, as shown in Fig. 5(c) and (d). For a larger block, but one which remains smaller than the size of the core, Fig. 5(e) and (f) show that the presence of the adiabatic block tends to "pull" the isotherms together thus preventing vertical heat conduction across the conduction dominant core. The vertical heat conduction across the square block of length L can be estimated as $Q_{cond} \sim k_f[T_{top} - T_{bottom}]$. It is clear that the effect of the increase in block size (L) is to cause $T_{top} \to T_H$ and $T_{bottom} \to T_C$ (as seen in Fig. 5a) thus increasing the wall heat transfer, as the lateral heat

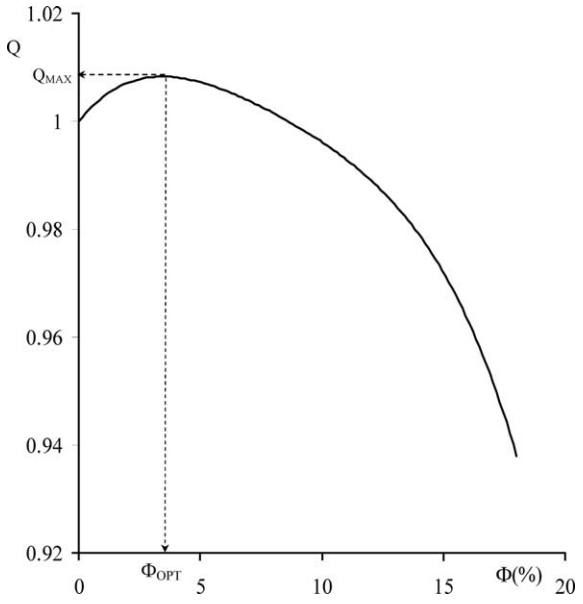

Fig. 6. Variation of the heat flux enhancement parameter, Q, with the adiabatic block size (Φ) for $Ra = 10^4$, and $Pr = 0.71$.

transfer "prevented" by the block has to leave the enclosure across the side walls. However this happens only until $L \sim W_{MAX}$ (Fig. 5(i) and (j)) and beyond this as $L > W_{MAX}$ (Fig. 5(k) and (l)), the adiabatic block continues to prevent a larger contribution of lateral conduction from top to bottom. Nevertheless, it also removes a portion of the convecting fluid itself, resulting in the loss of a wall-to-wall convection enthalpy of greater magnitude than the vertical heat conduction that is prevented from Case 1. The net effect is thus a decrease in the wall heat transfer. The variation of the rate of heat transfer with Φ for the above situation is summarized in Fig. 6, where the ordinate is defined using Eq. (10) while the abscissa is Φ, $(=L^2)$. The maximum heat transfer enhancement Q_{MAX} occurs when Φ Φ_{OPT}. This optimum corresponds to a block size, L, where $\Phi = L^2$, which is such that $L \sim W_{MAX}$; this result appears to be independent of values of Ra and Pr.

The effect of an optimum block size on the isotherms and streamlines is shown in Fig. 7 for $Pr = 0.071$ and $Ra = 10^6$. As the conduction dominant core of $Pr = 0.071$ is governed by a single length scale (since $B_{MAX} \sim W_{MAX}$), the vertical heat conduction effect is minimized in Fig. 7(b) by using a square block of size $L_{OPT} \sim W_{MAX}$. Observe in this situation of $B_{MAX} \sim W_{MAX}$, the square block of L_{OPT} does not invade and replace the originally convecting fluid in Case 1 ((a) and (c) in Fig. 7). However, the isotherms are seen easily to be more compressed when the block is present than when it is absent.

The requirement of a single length scale to delineate the core, as is the case above when $Pr = 0.071$, is not true when $Pr = 7.1$, as shown in Fig. 8, where the core is governed at least by two length scales ($B_{MAX} > W_{MAX}$) and is clearly rectangular. A square block of single length scale L would invade and replace the originally convecting fluid in the transverse direction (core governed by W_{MAX}), before it can replace the conduction dominant core in the longitudinal direction (core governed by B_{MAX}). A better block shape for this situation to prevent vertical heat conduction could be of rectangular cross section. However, for

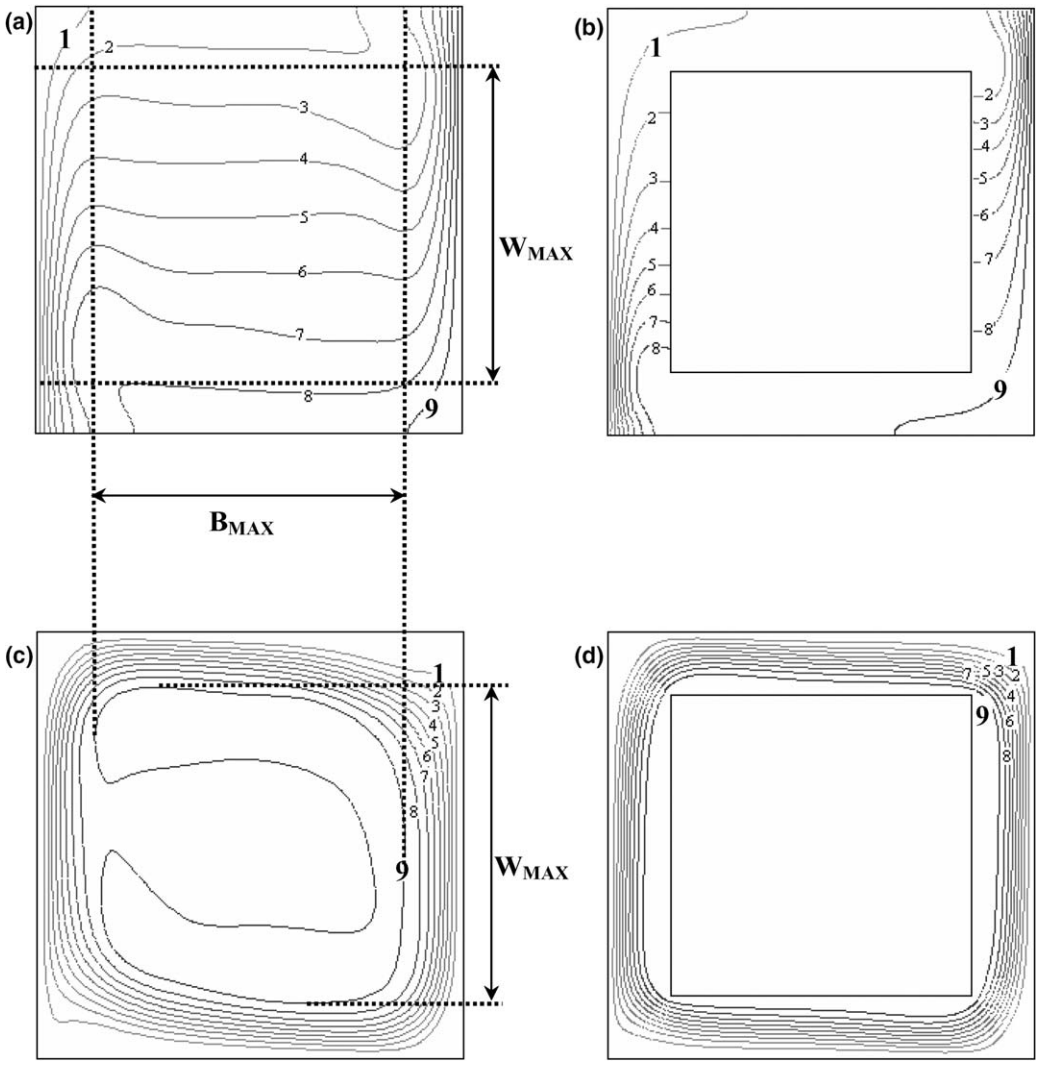

Fig. 7. Isotherms and streamlines respectively for $Ra = 10^6$ and $Pr = 0.071$: Case 1 in (a), (c) and Case 2 with Φ_{OPT} in (b), (d).

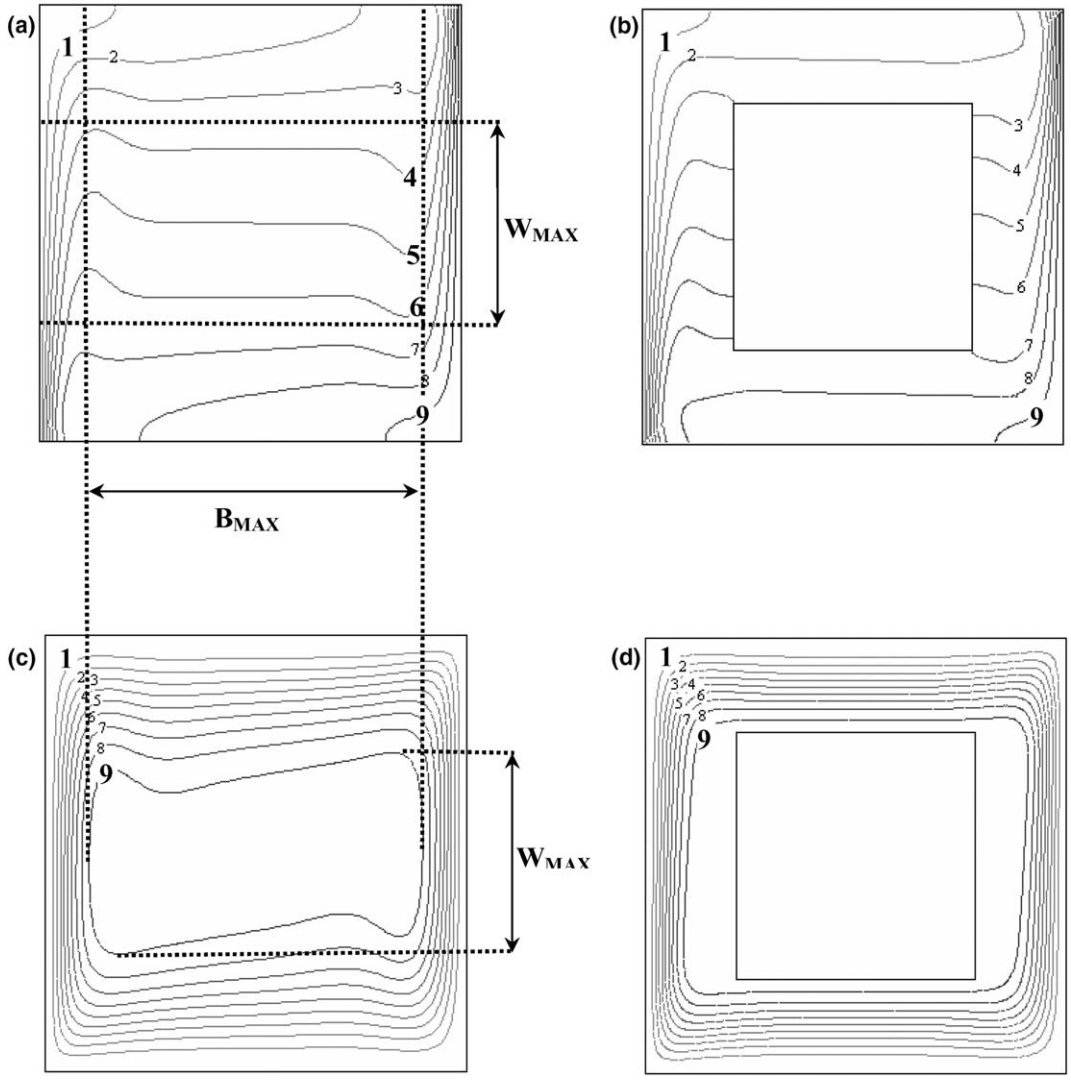

Fig. 8. Isotherms and streamlines respectively for $Ra = 10^6$ and $Pr = 7.1$ Case 1 in (a) and (c); Case 2 for Φ_{OPT} in (b) and (d).

completeness and clarity we restrict ourselves to using blocks with square cross section. Strong vertical heat conduction effects can be seen in Fig. 8(a), from the horizontal nature of the streamlines, most of which is prevented by insertion of the adiabatic block, as can be seen from Fig. 8(b). The isotherms have again been compressed and thus the vertical heat conduction prevented. Fig. 8(c) shows that there is a certain amount of distortion in the streamlines, and that the core is not perfectly rectangular. Insertion of the block forces the flow into the "channel" between the block and the enclosure walls.

Fig. 9 shows the effect of different values of Ra on the heat transfer enhancement and the corresponding optimum block size required for a $Pr = 0.071$ fluid. It is shown that Φ_{OPT} increases with increasing Ra because of the increase in the size of the stagnant fluid core in Case 1 as shown by the behavior of the streamlines in Fig. 3. The increase in Φ_{OPT} may also be explained by appealing to the expression for the thickness of the steady-state thermal boundary layer coating the vertical walls, $\delta_T \sim HRa^{-1/4}$ (from p. 224,

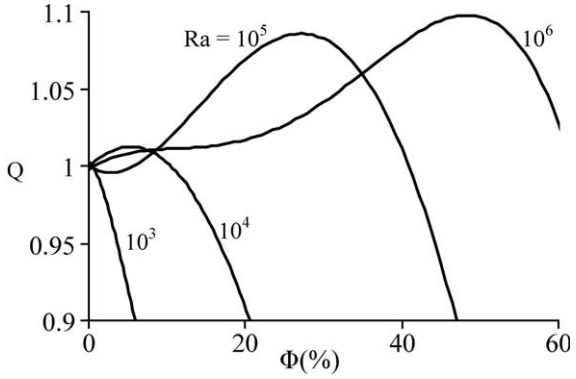

Fig. 9. Variation of heat flux enhancement parameter, Q, with adiabatic block size, Φ, for different values of Ra for $Pr = 0.071$.

[4]), which predicts a decrease in the δ_T or an increase in the conduction dominant core for increasing Ra. Therefore, the increase in the core size for $Pr = 0.071$, defined by Eq. (11) and governed by a single length scale ($B_{MAX} \sim$

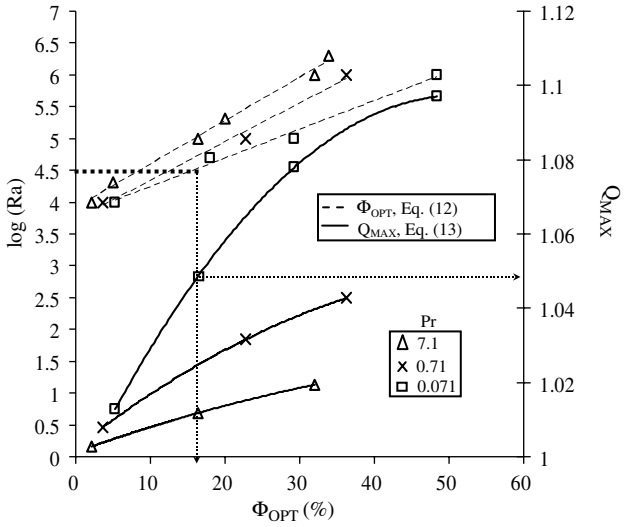

Fig. 10. Variation of the optimum block size Φ_{OPT} and maximum heat flux enhancement Q_{MAX} with Ra for different values of Pr.

W_{MAX}) as seen from Table 3, promotes more vertical heat conduction between the hot top layer of the core and the cold bottom layer. The prevention of this heat transfer needs a larger Φ_{OPT} and hence an increased heat transfer as well.

Fig. 10 summarizes the results of the numerical simulations for the three different Pr (0.071, 0.71 and 7.1) and for the range $10^3 \leqslant Ra \leqslant 10^6$. The abscissa corresponds to the Φ_{OPT} values, while the ordinate on the left side is for $\log(Ra)$ and on the right side is for Q, the heat transfer increase due to the presence of the block. For a chosen Ra (left-side ordinate), the Φ_{OPT} (abscissa) is located on the dashed-lines for each Pr value. Once this Φ_{OPT} is located, the corresponding Q_{MAX} value (right ordinate) may be obtained from the continuous curves. This exercise is shown in dotted line for $Ra = 10^{4.5}$ in Fig. 10. For a given Ra, from Fig. 10, it can be observed that as Pr decreases, both the Φ_{OPT} and the corresponding Q_{MAX} increases. From the values for W_{MAX} in Table 3 and the explanation for Fig. 9 it is obvious that the value of Φ_{OPT} for $Pr = 0.071$ would be the largest for a given Ra value, which is corroborated in Fig. 10. Since the $Pr = 0.071$ case allows the maximum size for Φ_{OPT} in Case 2, without replacing the originally convecting fluid of Case 1 (as $L_{OPT} \sim B_{MAX} \sim W_{MAX}$), Q_{MAX} is highest for all Ra values in this case, which is also evident from the results of Fig. 10. On decreasing Pr from 7.1 to 0.71, W_{MAX} increases as seen in Table 3, which prescribes in turn an increase in Φ_{OPT} and Q_{MAX}, as seen in Fig. 10. Further, for a given optimum core size Φ_{OPT} (i.e., δ is fixed), for decreasing Pr, the thermal diffusivity of the fluid increases, leading to a total increase in the vertical heat conduction across the conduction dominant core (as $Q_{cond} \sim k_f[T_{top}-T_{bottom}]$) of identical average temperature (recall, that the natural convection is across a fixed wall ΔT). Thus the prevention of this heat transfer using the adiabatic block increases the overall wall heat transfer increase. Hence, as seen in Fig. 10, Q_{MAX} increases with decreasing values of Pr.

Table 4
Values of curve-fit constants of Eqs. (12) and (13)

Pr	A_1	A_2	B_1	B_2	B_3	R^2 for Eq. (12)	R^2 for Eq. (13)
0.071	0.0452	3.7843	−0.00003	0.003495	0.9999	0.9888	0.9936
0.71	0.0608	3.7319	−0.00002	0.001717	1.0009	0.9903	0.9986
7.1	0.0687	3.9022	−0.00006	0.0008	1.0007	0.9942	0.9987

Table 5
Comparison between the values of L and W_{MAX} for several Ra and Pr

Ra	$Pr = 0.071$		$Pr = 0.71$		$Pr = 7.1$	
	W_{MAX}	L_{OPT} (Eq. 12)	W_{MAX}	L_{OPT} (Eq. 12)	W_{MAX}	L_{OPT} (Eq. 12)
10^4	0.284	0.218	0.252	0.209	0.248	0.119
10^5	0.574	0.518	0.452	0.456	0.31	0.399
10^6	0.746	0.7	0.656	0.610	0.464	0.552

The numerical data in Fig. 10 are curve-fits from which predictive correlations relating the Φ_{OPT} to the Ra and Pr of the convection situation and the corresponding maximum heat transfer Q_{MAX} are proposed of the form

$$\Phi_{OPT} = \frac{1}{A_1}[\log(Ra) - A_2] \tag{12}$$

$$Q_{MAX} = B_1\Phi_{OPT}^2 + B_2\Phi_{OPT} + B_3 \tag{13}$$

where the coefficients depend on Pr and are listed in Table 4, along with the R^2 values to indicate the goodness of the curve-fit employed in Fig. 10. The correlations in Eqs. (12) and (13) are found to predict the numerical results to within ±3%. In Table 5, the values of L predicted from Eq. (12) are compared with the values of W_{MAX} given in Table 3 and are found to be in good agreement. This supports our earlier observation that, whenever $L < W_{MAX}$ (where $\Phi = L^2$), there is heat transfer enhancement across the enclosure and at $L \sim W_{MAX}$, an optimum (maximum) in heat transfer is reached.

6. Conclusions

It is observed from the detailed simulations that the prevention of vertical heat conduction between the hot fluid on the top and the cooler fluid at the bottom of the enclosure through the stagnant fluid core, increases the left-to-right rate of heat transfer, when compared with the no-adiabatic-block situation. However, for each Ra (and Pr), there exists an optimum block size, which is roughly equal to the conduction dominant core size of the no-block case, and which generates maximum wall heat transfer. For instance, when an adiabatic block of appropriate size ($\Phi_{OPT} \sim 50\%$) is inserted in an enclosure with naturally convecting fluid of $Pr = 0.071$, a heat transfer enhancement of 10% over the no-block case is observed for $Ra \sim 10^6$, which decreases progressively for other Ra and Pr values.

For a block size which is greater than this optimum block size, the wall heat transfer decreases as the increasing block size displaces the originally convecting fluid that carried greater enthalpy across the enclosure. We find that the rate of heat transfer increases with $\Phi = L^2$) when $L < W_{MAX}$. At $L \sim W_{MAX}$, an optimum (maximum) in heat transfer is reached, and as L increases further the rate of heat transfer decreases once more. These results are valid for values of Ra and Pr within the ranges considered. Useful and simple correlations predicting this optimum block size of square cross section and the corresponding maximum heat transfer as a function of Ra and Pr are proposed in Eqs. (12) and (13), which predict within $\pm 3\%$, the numerical results.

References

[1] S. Kakac, A. Aung, R. Viskanta (Eds.), Natural convection: fundamentals and applications, Hemisphere, 1985.

[2] K.T. Yang, Natural convection in enclosures, in: S. Kakac, R.K. Shah, W. Aung (Eds.), Handbook of Single Phase Convective Heat Transfer, Wiley, NY, 1987 (Chapter 13).

[3] B. Gebhart, Y. Jaluria, R.L. Mahajan, B. Sammakia, Buoyancy-induced flows and transport, Hemisphere (1988).

[4] A. Bejan, Convection Heat Transfer, second ed., Wiley & Sons, 1995.

[5] J.M. House, C. Beckermann, T.F. Smith, Effect of a centered conducting body on natural convection heat transfer in an enclosure, Num. Heat Transfer Part A 18 (1990) 213–225.

[6] A.A. Merrikh, A.A. Mohamad, Blockage effects in natural convection in differentially heated enclosure, J. Enhanced Heat Transfer 8 (1) (2001) 55–74.

[7] A.A. Merrikh, J.L. Lage, A.A. Mohamad, Comparison between pore level and porous medium model for natural convection in a non-homogeneous enclosure, in: Z. Chen, R.E. Ewing (Eds.), Fluid Flow and Transport in Porous Media: Mathematical and Numerical Treatment, 2001, pp. 387–396.

[8] A.A. Merrikh, J.L. Lage, Natural convection in an enclosure with disconnected and conducting solid blocks, Int. J. Heat Mass Transfer 48 (7) (2005) 1361–1372.

[9] J.Y. Oh, M.Y. Ha, K.C. Kim, Numerical study of heat transfer and flow of natural convection in an enclosure with a heat-generating conducting body, Num. Heat Transfer Part A 31 (1997) 289–304.

[10] M.Y. Ha, M.J. Jung, Y.S. Kim, Numerical study on transient heat transfer and fluid flow of natural convection in an enclosure with a heat-generating conducting body, Num. Heat Transfer Part A 35 (1999) 415.

[11] R.L. Fredrick, A. Valencia, Heat Transfer in a square cavity with a conducting partition on its hot wall, Int. Commun. Heat Mass Transfer 16 (1989) 347–354.

[12] A. Nag, A. Sarkar, V.M.L. Shastri, Natural convection in differentially heated cavity with a horizontal partition plate on the hot wall, Comput Methods Appl. Mech. Eng. 110 (1993) 143–156.

[13] E. Belgin, Natural convection in cavities with a thin fin on the hot wall, Int. J. Heat Mass Transfer 48 (2005) 3493–3505.

[14] S.V. Patankar, Numerical heat transfer and fluid flow, Hemisphere (1981).

[15] B.P. Leonard, A stable and accurate convective modeling procedure based on quadratic upstream interpolation, Comput. Methods Appl. Mech. Eng. 19 (1979) 59–98.

[16] G. de Vahl Davies, Natural convection of air in a square cavity: a bench-mark numerical solution, Int. J. Num. Methods Fluids 3 (1983) 249–264.

[17] A.A. Merrikh, J.L. Lage, Effect of distributing a fixed amount of solid constituent inside a porous medium enclosure on the heat transfer process, Proc. Int. Conf. Appl. Porous Media (2004) 51–57.